Available online at www.sciencedirect.com
ScienceDirect
Journal of Photochemistry and Photobiology A: Chemistry 195 (2008) 254–260
Journal of Photochemistry and Photobiology A:Chemistry
www.elsevier.com/locate/jphotochem

Quenching dynamics promoted by silver nanoparticles

I-Yin Sandy Lee *, Honoh Suzuki

Department of Chemistry, University of Toyama, 3190 Gofuku, Toyama 930-8555, Japan

Received 12 June 2007; received in revised form 26 September 2007; accepted 12 October 2007
Available online 22 October 2007

Abstract

We have studied fluorescence quenching by electron transfer between tris(2,2′-bipyridyl)ruthenium(II) complex and methyl viologen in solutions containing silver nanoparticles. The Stern–Volmer plot and transient absorbance indicate that both dynamic and static mechanisms are involved in the quenching. In the presence of silver nanoparticles, reverse saturable absorption at silver surfaces has promoted the quenching process by populating the excited triplet state of the donor species. Furthermore, the negatively charged silver particles are effective catalysts in attracting the cationic donor–acceptor pairs into the "sphere-of-action", which is the dominant mechanism for the static quenching.

Keywords: Nanoparticles; Electron transfer; Reverse saturable absorption; Sphere-of-action

1. Introduction

Electron transfer (ET) is the principal process involved in the photosynthesis that converts light to chemical energy [1]. It is also the core reaction in the power conversion for solar-energy plants. Reverse saturable absorption (RSA) is a nonlinear optical phenomenon occurring in light absorbers exposed to an intense radiation, in which the absorption is not saturated but enhanced due to the higher excited-state absorbance [2]. Thus, if combined with photo-induced ET processes, RSA can be potentially useful in promoting effective absorption and better utilization of light energy. In this work, we have studied a typical ET process between donor and acceptor dye molecules in solution, and by examining the effect of silver nanoparticles added to the solution, we have aimed at elucidating the role played by RSA occurring on the surface of the nanoparticles.

In view of the importance of ET and to achieve high efficiency, the physical chemistry of ET has been extensively studied. It is well known that, for the reaction to initiate, the system has to overcome an energy barrier of $\Delta = I_D - E_A$, where I_D is the ionization potential of the donor and E_A is the electron affinity of the acceptor [3]. The transfer process is also subject to other factors, such as steric effects along the transfer pathway, direct Coulomb interactions between the donor and acceptor, and long-ranged electrostatic interactions characterized by the ionic strength [4]. An essential parameter in controlling the rate of ET processes is the donor–acceptor distance [5,6], because the transfer rate decreases exponentially with the increasing distance. In addition, efficient escaping from the solvent cage is required for the rapid charge-separation of the redox pair [7,8].

A number of schemes have been developed to cope with these parameters and proved effective in increasing ET efficiency. One of the successful methods is to incorporate the ET pairs into catalyst media and heterogeneous systems. For the donor–acceptor pair used in this work, tris(2,2′-bipyridyl)ruthenium(II) complex (TBR) and methyl viologen (MV^{2+}), media such as cellulose [8], zeolite [9], and zirconium phosphates [10] have been studied. Because the electron transfer between TBR and MV^{2+} is known to suffer from rapid charge-recombination, these media are employed mainly to counteract this problem. For example, various structural conformations of zeolite have been designed to bind TBR or MV^{2+} at specific sites, so that the interaction distance and the diffusional motion are under control. In such a manner, the media can be used to steer the ET interactions in favor of charge-separation [9]. In the case of cellulose [8], the media was kept at the freezing temperature to attain a totally tunneling-mediated electron transfer.

In addition to serving as host cages and distance fixers, heterogeneous media can also play a more active role in the ET process. Semiconductor particles such as TiO_2 are known to actually

* Corresponding author. Tel.: +81 76 445 6612; fax: +81 76 445 6549.
E-mail address: islee@sci.u-toyama.ac.jp (I.-Y.S. Lee).

1010-6030/$ – see front matter © 2007 Elsevier B.V. All rights reserved.
doi:10.1016/j.jphotochem.2007.10.009

participate in photochemical ET reactions [11]. In our previous study of TBR emission in silver nanoparticle solutions, we found strong interactions between the dye and the nanoparticle surface. It turned out that RSA of the nanoparticle, originating from laser-induced free-carrier absorption, contributed to the enhancement in the TBR emission [12]. It is likely that ET processes in heterogeneous systems may benefit from this sort of nonlinear optical process as well.

In the case of ionic donor–acceptor pairs, nanoparticle surfaces raise another issue: the electrostatic surface potential. Charge-separation due to surface potentials has been demonstrated in colloidal SiO_2 systems, where the Coulombic repulsion keeps the ET products apart from recombination [13]. Charge effects are also the origin of a greater efficiency of ET found in alumina-coated silica suspensions; anionic ET reactants are adsorbed on the positively charged surfaces of silica particle, resulting in an increase in the ET yield [14]. Such Coulombic interactions are also expected to play an important role in ET reactions in our nanoparticle suspensions.

2. Experimental

2.1. The preparation and characterization of TBR–MV^{2+}

Tris(2,2′-bipyridyl)ruthenium(II) chloride hexahydrate $[Ru(bpy)_3]Cl_2{\cdot}6H_2O$ and methyl viologen dichloride hydrate were purchased from Aldrich and used without further purification. All solutions were prepared with distilled water. Silver nanoparticles were prepared by mixing a silver nitrate solution (0.6 mM) with a sodium tetrahydroborate solution (0.1 mM), followed by the addition of silver nitrate (0.3 mM) and ascorbic acid (0.4 mM) to give a solution of silver nanoparticles of 40 nm in diameter [15]. The resulting particle suspension stayed stable without stabilizing surfactants or ligands for several days. The absorption spectra were measured with a Shimadzu UV-160 spectrophotometer. For the detection of possible laser-induced degradation, the spectra were obtained before and after the emission measurement; for all samples used in this work, no significant change was observed. Prior to each emission measurement, a TBR solution (0.182 mM) was freshly prepared by mixing the ruthenium complex with either water or the nanoparticle suspension in a 1 cm glass cell. The solution was purged in argon for 5 min for oxygen removal. The emission spectra were recorded along with the additions of MV^{2+} up to the final concentration of 2.5 mM.

2.2. The excitation and detecting system

The excitation source was a frequency-doubled, Q-switched Nd: yttrium–aluminum–garnet (YAG) laser ($\lambda = 532$ nm) with a pulse width of 5 ns (Continuum Surelite I-10). Time-integrated emission was collected with an optical-fiber CCD spectrometer (Ocean Optics CHEM2000). Single-wavelength transient absorbance changes following the laser-pulse excitation were obtained using a Xe flash lamp (Hamamatsu C5604) as the probe light and a detecting system composed of an optical fiber, a monochromator (Optometrics DMC1-03), a photomultiplier tube (Hamamatsu R1477-06), and an oscilloscope (Tektronix TDS-3032).

Time-gated transient absorption spectra were measured with an optical-fiber spectrograph (CVI CMSP110) and an image-intensified CCD camera (Hamamatsu V4183U-NESA/C6588-MOD), which enabled us to measure spectrograms at a short gating time (and thus a small total number of incident photons) down to the photon-counting mode. The gating duration of the intensifier was controlled with a home-built high-voltage pulse generator, which used either avalanche transistors (Zetex ZTX415) or ultrafast high-voltage MOSFETs (Supertex VP/VN 0550/2106) as a low-cost solution to the high-speed high-voltage electronic gating down to 5 ns. The CCD image from the output slit of the spectrograph was converted to a one-dimensional spectrogram by pixel integration. The wavelength and the device sensitivity were calibrated with a NIST-traceable standard Hg light source. All the instruments were synchronized and controlled with a delay generator (SRS DG535).

2.3. Data processing

The light pulse from the probing flash lamp was long enough (ca. 1 μs) to cover the time scale of our interest, and found to have a stable temporal and spectral profile; however, its jitter relative to the triggering signal was large (200 ns typical) and its overall intensity was fluctuating (5% typical). Accordingly, for the time-resolved absorbance to be accurately computed, the reference light intensity as a function of time, $I_0(t)$, had to be determined at each flash. Because our system was a 'single-beam' one, i.e., not capable of the simultaneous monitoring of two intensities $I_0(t)$ and $I(t)$, the former was obtained by adjusting the standard temporal profile $I_{0,\mathrm{std}}(t)$ to each flash: $I_0(t) = f\, I_{0,\mathrm{std}}(t-\delta)$, where δ is the jitter and f the correction (normalization) factor for the overall intensity. The two parameters, δ and f, were in turn determined by the least-square fitting, $I(t) = f\, I_{0,\mathrm{std}}(t-\delta)\ 10^{-\mathrm{A}}$, in the time region where the absorbance should be constant and equal to the static value (A), i.e., before the laser-pulse irradiation and after a long delay time. The standard profile was separately determined by the least-square optimization of 30 flashes before each run. The analysis was performed with a C program and a Python script written by us. For the calculation of the transient absorption spectra, the method was extended to incorporate the wavelength dependence in a straightforward manner. The validity and reliability of the above single-beam approach was confirmed by the fact that data sets with very different jitters gave practically identical results of the transient absorbance. All the laser experiments were carried out at the pulse energy of 73 mJ unless specified otherwise.

3. Results and discussion

3.1. Emission of TBR–MV^{2+}

Fig. 1a and b shows the single-shot emission spectra of TBR–MV^{2+} solutions with and without silver nanoparticles.

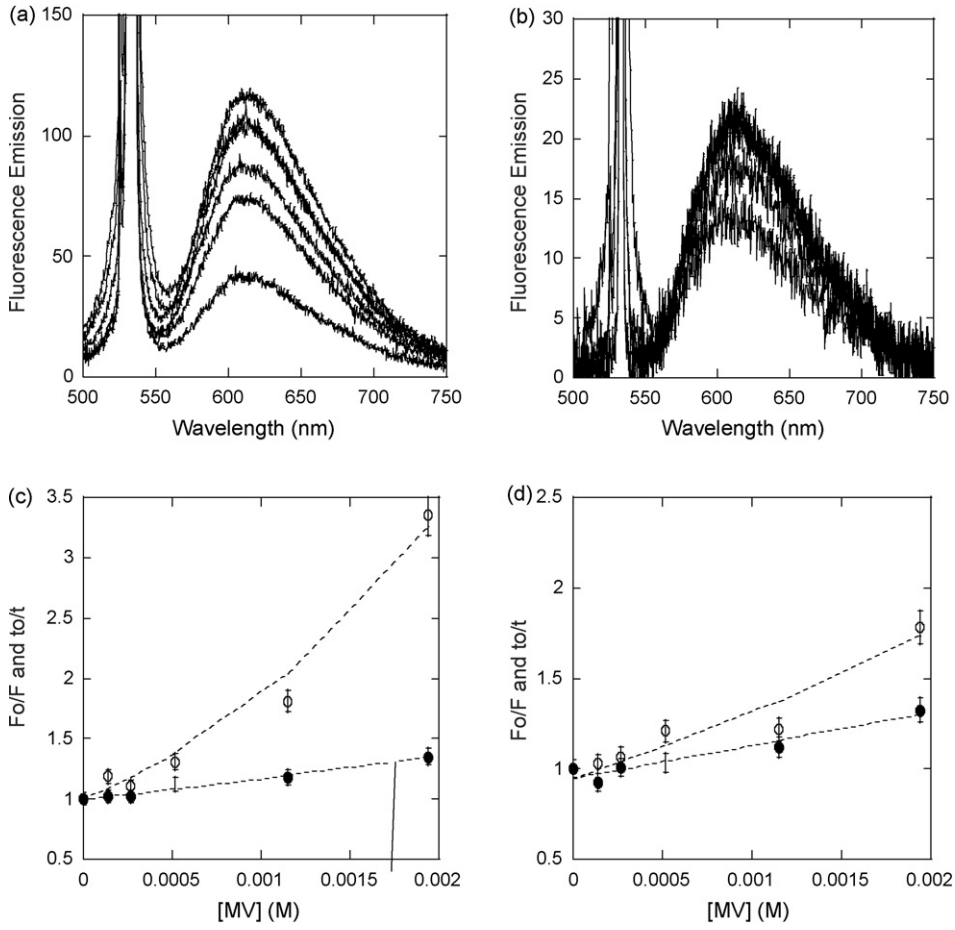

Fig. 1. Emission spectra of TBR solutions (0.182 mM): (a) with nanoparticles (Ag 13.2 μM) and (b) without nanoparticles. MV^{2+} concentrations: 0, 0.138, 0.269, 0.517, 1.148 and 1.938 mM (from top to bottom). (c) The relative emission intensity, F_0/F (◯), and lifetime, t_0/t (●), as functions of the MV^{2+} concentration in nanoparticle solutions. (d) The ratios of F_0/F and t_0/t in water. Dashed lines in (c) and (d) are curve fittings by the sphere-of-action (F_0/F) and the Stern–Volmer equation (t_0/t).

In both cases, the emission band extends from 550 to 750 nm, whereas the intense scattering at 532 nm is from the excitation source. Enhancement of both the TBR emission and the scattering by the nanoparticles is evident. Our previous study on the TBR-nanoparticle system [12] showed that the enhanced scattering is not linear (e.g., Rayleigh) but nonlinear in pulse-energy dependence, and that the enhancement of TBR fluorescence is mostly attributable to the nonlinear absorption effect, i.e., RSA, at the surfaces of silver nanoparticles. In this system, the RSA effect has its origin in free-carrier absorption of silver nanoparticles (not the transient absorption of TBR), where the free carriers originate from the intraband conduction electrons or the surface plasmon resonance [12]. As for quenching, the nanoparticles also have a significant effect: at the same concentration of MV^{2+}, the presence of the nanoparticles induces stronger quenching. We have summarized the emission intensity and lifetime in Fig. 1c and d, where the relative values, F_0/F and t_0/t, are plotted against the MV^{2+} concentration.

Generally speaking, the fluorescence quenching by ET processes can be analyzed via two mechanisms: dynamic and static. The yield in dynamic (collisional) quenching is linearly related to the quencher concentration, as described by the Stern–Volmer equation [4],

$$\frac{F_0}{F} = 1 + \kappa_q t_0 [MV^{2+}], \tag{1}$$

where κ_q is the quenching constant and $[MV^{2+}]$ the quencher concentration. This mechanism usually assumes electron transfer from excited-state donors, and thus t_0/t is equal to F_0/F. On the other hand, for static quenching, F_0/F also increases with $[MV^{2+}]$, but t remains unchanged, i.e., $t_0/t = 1$. In this case, a ground-state equilibrium between intact donor species and non-fluorescent ones is assumed, which is caused by either complex formation or perfect quenching within the so-called "sphere-of-action" [4]. We can readily see in Fig. 1c and d that the t_0/t plot is neither equal to F_0/F nor unity. The upward curvature of the F_0/F plot (◯), especially evident in Fig. 1c, suggests that both dynamic and static quenching mechanisms are operating. Since the t_0/t plot (●) is linear, we may estimate the quenching constant κ_q for the dynamic mechanism based on Eq. (1). It turns out that κ_q is equal to $(3.25 \pm 0.08) \times 10^8\ M^{-1}\ s^{-1}$ ($t_0 = 550 \pm 15$ ns) in the nanoparticle solutions, and $(3.45 \pm 0.09) \times 10^8\ M^{-1}\ s^{-1}$ ($t_0 = 530 \pm 15$ ns) in water. These values are comparable to but somewhat smaller than the literature value of

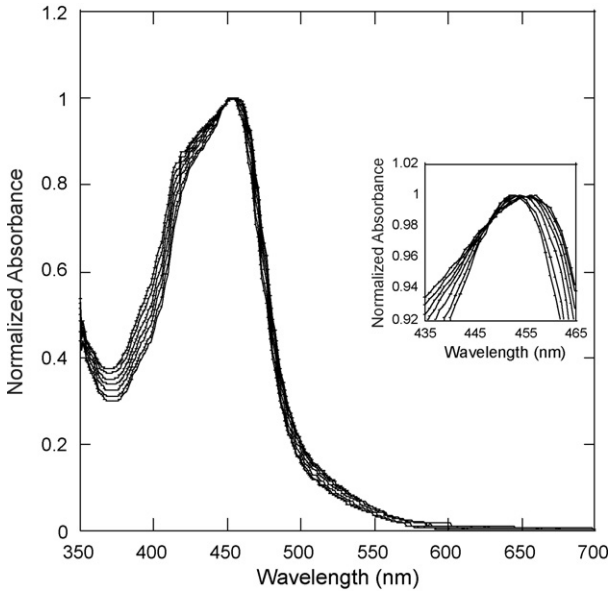

Fig. 2. Normalized absorption spectra of TBR solutions with nanoparticles. The inset shows blue-shifting and band narrowing of the spectra with the addition of MV^{2+} and the dilution of TBR. MV^{2+} concentrations: 0.055, 0.111, 0.270, 0.517, 0.954, 1.653 and 2.514 mM; and TBR concentrations: 0.182, 0.179, 0.174, 0.167, 0.154, 0.133, 0.108 mM (broad to narrow).

$(4.6 \pm 0.2) \times 10^8\ M^{-1}\ s^{-1}$ [16]. It is noted that κ_q in nanoparticle solutions is just slightly smaller than that in water, i.e., the dynamic quenching is quite similar in both cases. Decrease in the quenching rate, however, seems common in heterogeneous environments, where ET takes places in a relatively restricted space [10].

In many instances of static quenching, complex formation between donor–acceptor pairs is indicated by the appearance of one or more new bands in the absorption spectrum. In our case, the absorption spectra of TBR–MV^{2+} solutions, with or without nanoparticles (Fig. 2), show no obvious sign of extra bands. MV^{2+} itself has very weak absorption in this region, but we expect that, if TBR–MV^{2+} complexes formed as a major species, there should have been significant changes in the TBR absorption band. This is not the case. Although, there is minor but appreciable blue-shifting and band narrowing (inset of Fig. 2) with the addition of MV^{2+} (and thus the dilution of TBR) in the nanoparticle solutions, we ascribe them to the concentration dependence of the TBR spectrum; a similar trend has been observed in the spectra of TBR solutions without silver particles as the TBR concentration is varied. Kim and Mallouk reported spectral shifts in the emission of TBR adsorbed onto zeolites, and claimed that the shift became noticeable as the loading of TBR on zeolites approached to monolayer coverage [9]. Because the formation of monolayer coating of TBR on the nanoparticle surface has been verified earlier [12], we speculate that the observed concentration dependence of the TBR absorption band may, at least partially, result from the change in the ground state of TBR adsorbed on the silver surface at a high-coverage ratio. The observed spectra, the stability of the solutions, and the inspection by optical microscopy also indicate that aggregation of the silver particles is minor, if any, in the fresh solutions used in our experiment. Accordingly, we propose the sphere-of-action as a plausible cause for the static quenching in our system.

3.2. Transient absorption of TBR–MV^{2+}

3.2.1. RSA effects

The transient absorption is helpful in revealing the quenching dynamics. Fig. 3 shows the transient absorption spectra (the image-intensifier gate duration = 50 ns) of TBR solutions, observed at the 90-ns delay after the 5-ns laser-pulse excitation. This delay time has been chosen so that possible complications due to instantaneous (<1 ns) laser-induced events (such as free-carrier absorption) can be avoided. In spite of noises due to the short gating time, the absorption change shows a clear peak at 370 nm in the nanoparticle solution; it is assigned to the absorption of triplet state of $[Ru(bpy)_3]^{2+}$ ($^3Ru^*$) [17]. This band is absent in the solution without nanoparticles. Accordingly, a significant $^3Ru^*$ population is created only when the nanoparticles are present. The result highlights the RSA effect at the silver surfaces, which may help to populate $^3Ru^*$ states through the energy coupling with the transition dipole of $[Ru(bpy)_3]^{2+}$ [12].

The transient absorption is more pronounced at a higher energy of excitation. Fig. 4 shows the transient absorption at 370 nm, at the pulse energies of 73 and 120 mJ. In the presence of nanoparticles, the absorption change is enhanced at the higher excitation energy (Fig. 4a); the normalization by the pulse energy (inset) reveals nonlinear nature of the enhancement, i.e., it is more than that expected from simple proportionality. In the case without nanoparticles, on the other hand, the transient absorbance is small at both energies, and the pulse-energy dependence is not as clear (Fig. 4b). As for the decay rate, the pulse-energy dependence is small in both cases; however, when the concentration of MV^{2+} in the nanoparticle solution is varied, subtle but significant changes are seen, as is discussed below.

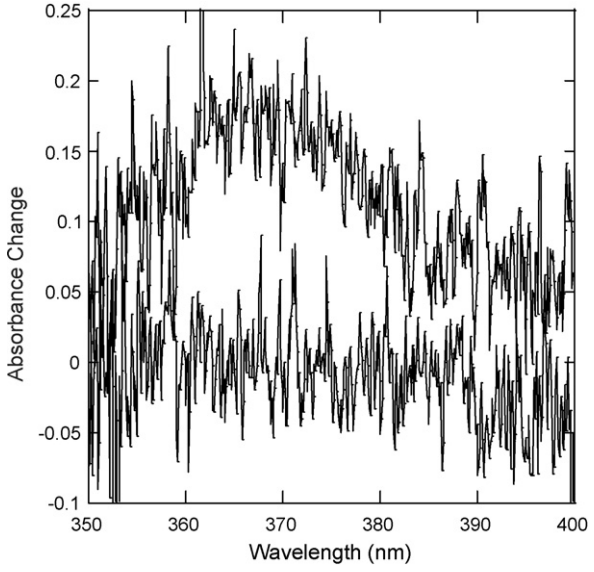

Fig. 3. Transient absorbance spectra of TBR solutions (0.182 mM) at the delay time of 90 ns after the laser-pulse excitation: with nanoparticles (Ag 13.2 μM) (top), and without nanoparticles (bottom).

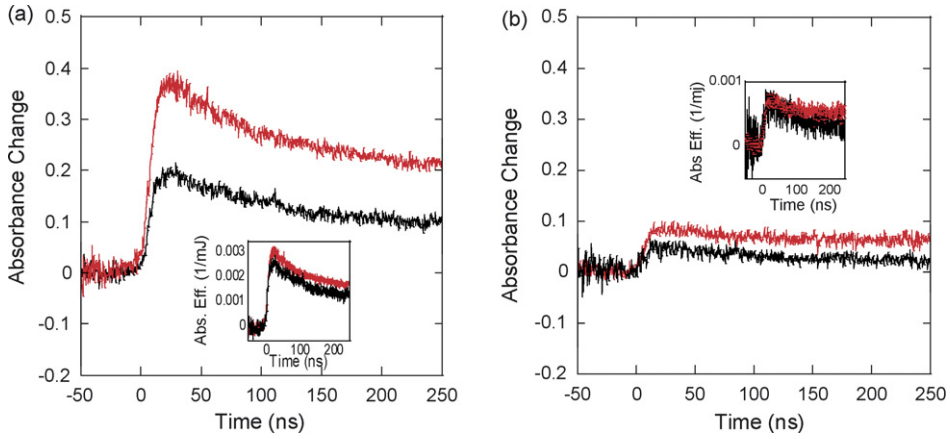

Fig. 4. Time-resolved absorbance change at 370 nm for TBR (0.176 mM) and MV^{2+} (0.159 mM) in (a) nanoparticle and (b) aqueous solutions, with the excitation pulse energy of 120 mJ (red) and 73 mJ (black). The insets show the normalized absorbance changes (per millijoule of excitation energy) in each case.

Fig. 5 shows transient absorption (semi-log) plots at 370 nm with the MV^{2+} concentration varied. In the absence of quenchers (Fig. 5a), it is characterized by a step-like function with a long lifetime (>200 ns); here the ^{3}Ru* state ($\varepsilon = 1.3 \times 10^4\,M^{-1}\,cm^{-1}$) dominates, which is more absorbing than the TBR ground state ($\varepsilon = 4.1 \times 10^3\,M^{-1}\,cm^{-1}$) [18]. With the addition of MV^{2+} (Fig. 5b), a sharp feature newly appears at the initial stage (0–50 ns). We have assigned this to the formation of MV^{2+} radicals, which are even more absorbing at 370 nm ($\varepsilon = 2.1 \times 10^4\,M^{-1}\,cm^{-1}$) [19]. This component only lasts for 20–30 ns, and then disappears when the electrons have transferred back to the donors (recombination). As the MV^{2+} concentration further increases, the intensity of the short-lived component first increases (Fig. 5c), then starts decreasing (Fig. 5d), and finally disappears, leaving the long-lived component only (Fig. 5e and f). At these higher quencher concentrations, the sphere-of-action quenching mechanism predominates (see below), so that the radicals may quickly disappear without diffusion or accumulation. As for the solutions without nanoparticles, the transient absorption always retains the step-like feature as in Fig. 5a, regardless of the quencher concentration (data not shown).

It is also noted that both the long and short-lived components in the nanoparticle solutions are similarly enhanced at the higher excitation energy (Fig. 4a). It implies a high correlation between RSA and ET: the number of MV^{2+} radicals that have formed via ET is proportional to the number of ^{3}Ru* states created by RSA effects. This demonstrates the usefulness of RSA in the enhancement of ET processes. Without nanoparticles, high-excitation energies may induce absorption saturation, and thus may not necessarily lead to the ET enhancement.

3.2.2. Sphere-of-action

The modified form of the Stern–Volmer equation that incorporates the contribution from the sphere-of-action mechanism is

$$\frac{F_0}{F} = (1 + \kappa_q t_0[MV^{2+}])\exp([MV^{2+}]\upsilon), \qquad (2)$$

where υ is the volume of the sphere [4]. The right hand side involves both the linear term for the dynamic quenching and the exponential term for the sphere-of-action, indicating that, the larger the sphere volume is, the more efficient the quenching will be. It assumes a Poisson distribution in space and that the quenching is guaranteed if one or more quenchers are inside the sphere around the donor at the moment of excitation; the quenching will always take place before the ET couple diffuses apart, which results in the quenching probability of unity [4].

We have evaluated the sphere volume by fitting our data to Eq. (2) using the value of κ_q (dynamic) determined from Eq. (1). The resulting quenching volume in the nanoparticle solutions ($\upsilon = 765 \pm 15\,nm^3\,molecule^{-1}$) turns out to be three times larger than that in water ($\upsilon = 250 \pm 8\,nm^3\,molecule^{-1}$). These values correspond to the quenching radii of 5.7 nm in the nanoparticle solutions and 3.9 nm in water, respectively, and reflect a greater chance for the donor to encounter quenchers in the presence of nanoparticles. The relation of this dimension to our nanoparticle diameter (40 nm) is, however, not obvious.

The concept of the quenching sphere is a useful, but rather vaguely defined one; in reality, it may represent a statistical combination of various mechanisms and environmental factors, rather than the literal dimensions. Perrin has originally defined the quenching radius as the sum of the radii of the reactants [20]. According to Colon et al. [10], however, quenching via electron transfer, instead of energy transfer as it was first proposed [21], can occur over some distance longer than the radius sum, typically 1.0 nm [22]. In the present system, the quenching via energy transfer is unlikely because the excited states of MV^{2+} lie higher than the ^{3}Ru* state [23]; however, the surface charge of the nanoparticles can attract the ionic quenchers, resulting in a non-Poissonian distribution and a larger apparent (effective) quenching volume. This possibility is briefly considered below.

3.2.3. Surface charge

Our nanoparticle solutions have a pH value of 7.4, which is higher than the isoelectric point (pI = 4–6), and thus the nanoparticle surfaces are negatively charged [24,25]. Accordingly, the

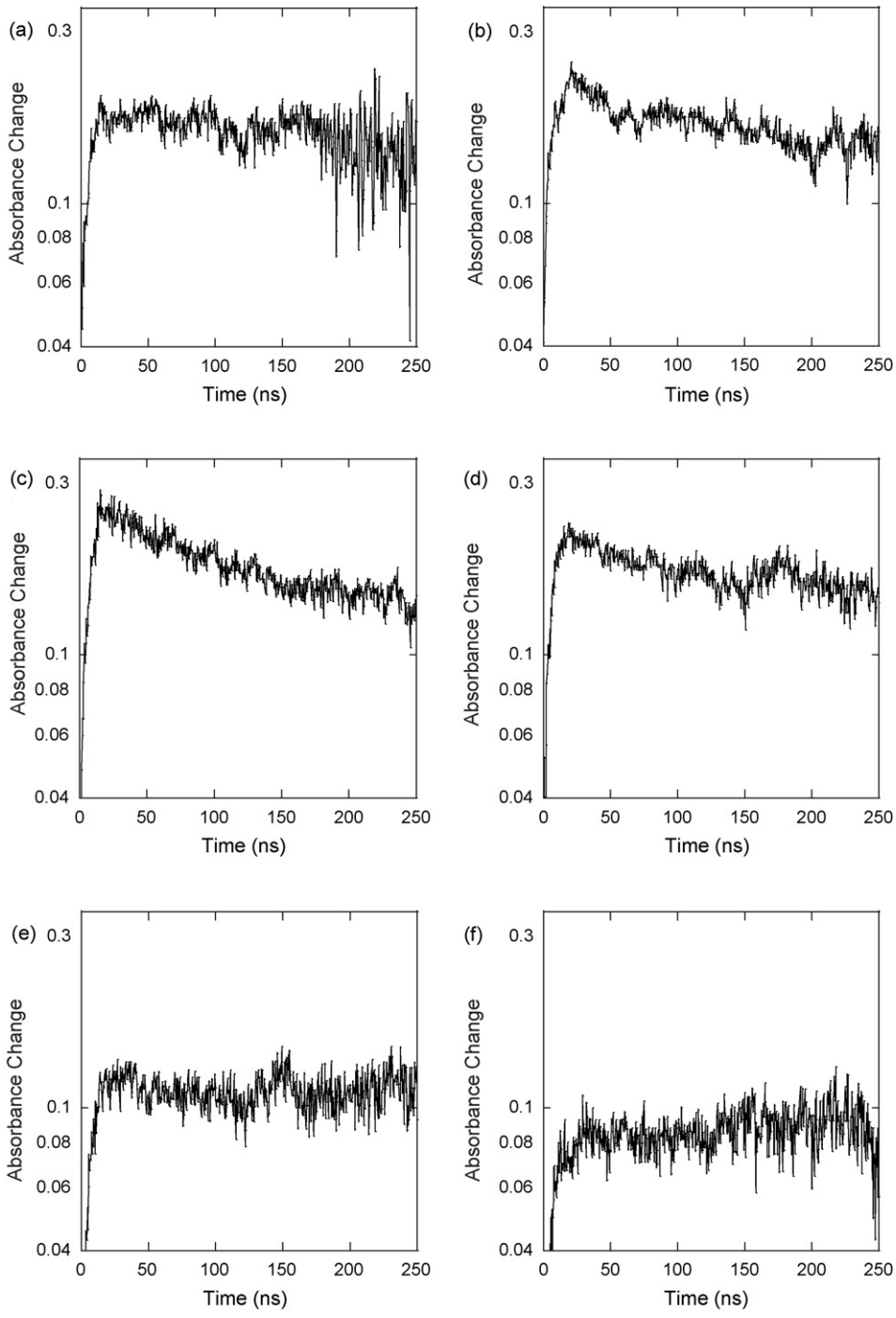

Fig. 5. Time-resolved absorbance change at 370 nm of TBR solutions (0.182 mM initial) containing nanoparticles (Ag 13.2 μM initial), with the excitation pulse energy of 73 mJ. The absorbance change is plotted in a logarithmic scale. MV^{2+} concentration: (a) 0 mM, (b) 0.111 mM, (c) 0.270 mM, (d) 0.517 mM, (e) 1.653 mM, and (f) 2.514 mM.

cationic ET reactants may deviate from random distribution and tend to populate more in the vicinity of the nanoparticle surfaces. It may involve not only physical and chemical adsorption (monolayer coverage) but also a statistical spatial distribution that is analogous to the Debye cloud for both TBR and MV^{2+} species. This leads to a lower possibility of finding zero quencher inside the sphere-of-action than that for the Poisson distribution, and therefore, a larger effective quenching volume in Eq. (2).

The sphere-of-action mechanism, in general, promotes both forward (ET) and backward (recombination) reactions, and can result in minimal or no net charge-separation. The charge-separation within the sphere often takes place on a very short time scale, and may not be detected due to the limited time resolution of the instrument [26]. This explains why the fast transient component in Fig. 5 has eventually disappeared when the sphere-of-action becomes dominant. Therefore, in order to enhance the net ET efficiency by the RSA effect, we may need to carefully

choose experimental conditions, such as nanoparticle surface charges and quencher concentrations, for the recombination to be minimal.

4. Conclusion

The silver nanoparticles are found to greatly enhance the ET process between TBR and MV^{2+} in solution. Enhancement mechanisms are: (1) the extensive creation of TBR triplets by RSA on the nanoparticle surfaces and (2) the static quenching via the sphere-of-action that is enhanced by the surface charges. Both originate from surface interactions between the dyes and the silver nanoparticles, and they contribute substantially to the ET process of the adsorbed TBR–MV^{2+} pairs in a parallel manner. RSA leads to enhanced dynamic transfer by increasing the population of excited TBR states via free-carrier absorption of silver surfaces, which has been triggered by the incident laser field. On the other hand, greater static quenching (dominated by sphere-of-action) results from the Coulombic interactions between the ET pairs and the silver surfaces. These findings are expected to help the future design and strategy of building a new host structure for efficient photochemical and heterogeneous ET applications.

Acknowledgment

This work is supported by Grants-in-Aid for Scientific Research No. 17510086 from the Ministry of Education, Science and Culture of Japan.

References

[1] J.-L. Martin, J. Breton, A.J. Hoff, A. Migus, A. Antonetti, Proc. Natl. Acad. Sci. USA 83 (1986) 957–961.
[2] L.W. Tutt, S.W. McCahon, Opt. Lett. 15 (1990) 700–703.
[3] R.S. Mulliken, W.B. Person, Molecular Complexes, John Wiley & Sons, New York, 1969.
[4] J.R. Lakowicz, Principles of Fluorescence Spectroscopy, Plenum Press, New York and London, 1983, Chapter 9.
[5] C.C. Moser, J.M. Keske, K. Warncke, R.S. Farid, P.L. Dutton, Nature 355 (1992) 796–802.
[6] G.L. Closs, J.R. Miller, Science 240 (1988) 440–447.
[7] M.Z. Hoffman, J. Phys. Chem. 92 (1988) 3458–3464.
[8] B.H. Milosavljevic, J.K. Thomas, J. Am. Chem. Soc. 108 (1986) 2513–2517.
[9] Y. ll Kim, T.E. Mallouk, J. Phys. Chem. 96 (1992) 2879–2885.
[10] J.L. Colon, C.Y. Yang, A. Clearfield, C.R. Martin, J. Phys. Chem. 94 (1990) 874–882.
[11] P.V. Kamat, Chem. Rev. 93 (1993) 267–300.
[12] I-Y.S. Lee, H. Suzuki, K. Ito, Y. Yasuda, J. Phys. Chem. B 108 (2004) 19368–19372.
[13] I. Willner, J.W. Otvos, M. Calvin, J. Am. Chem. Soc. 103 (1981) 3203–3205.
[14] P.V. Kamat, W.E. Ford, J. Phys. Chem. 93 (1989) 1405–1409.
[15] S. Schneider, P. Halbig, H. Grau, U. Nickel, Photochem. Photobiol. 60 (1994) 605–610.
[16] J.R. Darwent, K. Kalyanasundaram, J. Chem. Soc., Faraday Trans. 2 77 (1981) 373–382.
[17] A. Merrins, C. Kleverlaan, G. Will, S.N. Rao, F. Scandola, D. Fitzmaurice, J. Phys. Chem. B 105 (2001) 2998–3004.
[18] N. Sutin, C. Creutz, in: M. Wrighton (Ed.), Inorganic and Organometallic Photochemistry, American Chemical Society, Washington, DC, 1978.
[19] T.W. Ebbesen, G. Ferraudi, J. Phys. Chem. 87 (1983) 3717–3721.
[20] F.C. Perrin, R. Acad. Sci., Paris 178 (1924) 1978–1980.
[21] N.J. Turro, Modern Molecular Photochemistry, University Science Books, Sausalito, 1991.
[22] T. Guarr, M. McGuire, S. Strauch, G. McLendon, J. Am. Chem. Soc. 105 (1983) 616–618.
[23] G.J. Kavarnos, Fundamentals of Photoinduced Electron Transfer, VCH Publishers, Inc., New York, 1993.
[24] V.V. Hardikar, D.V. Goia, E. Matijevic, Colloids Surf. A 159 (1999) 121–133.
[25] I. Arnaud, J.-P. Abid, C. Roussel, H.H. Girault, Chem. Commun. 6 (2005) 787–788.
[26] P.J. Wagner, in: A.A. Lamola (Ed.), Creation and Detection of the Excited State, Marcel Dekker, New York, 1971.